THE JOURNAL OF BIOLOGICAL CHEMISTRY VOL. 286, NO. 5, pp. 3935–3943, February 4, 2011

Hetero-oligomerization of Neuronal Glutamate Transporters*

Received for publication, September 22, 2010, and in revised form, November 29, 2010 Published, JBC Papers in Press, December 2, 2010, DOI 10.1074/jbc.M110.187492

Doreen Nothmann[‡§1], Ariane Leinenweber[‡§1], Delany Torres-Salazar[‡§1,2], Peter Kovermann[‡§], Jasmin Hotzy[‡§], Armanda Gameiro[¶], Christof Grewer[¶], and Christoph Fahlke[‡§3]

From the [‡]Institut für Neurophysiologie, Medizinische Hochschule Hannover, D-30625 Hannover, Germany, the [§]Zentrum für Systemische Neurowissenschaften, D-30559 Hannover, Germany, and the [¶]Department of Chemistry, Binghamton University, State University of New York, Binghamton, New York 13902

Excitatory amino acid transporters (EAATs) mediate the uptake of glutamate into neuronal and glial cells of the mammalian central nervous system. Two transporters expressed primarily in glia, EAAT1 and EAAT2, are crucial for glutamate homeostasis in the adult mammalian brain. Three neuronal transporters (EAAT3, EAAT4, and EAAT5) appear to have additional functions in regulating and processing cellular excitability. EAATs are assembled as trimers, and the existence of multiple isoforms raises the question of whether certain isoforms can form hetero-oligomers. Co-expression and pull-down experiments of various glutamate transporters showed that EAAT3 and EAAT4, but neither EAAT1 and EAAT2, nor EAAT2 and EAAT3 are capable of co-assembling into heterotrimers. To study the functional consequences of hetero-oligomerization, we co-expressed EAAT3 and the serine-dependent mutant R501C EAAT4 in HEK293 cells and *Xenopus laevis* oocytes and studied glutamate/serine transport and anion conduction using electrophysiological methods. Individual subunits transport glutamate independently of each other. Apparent substrate affinities are not affected by hetero-oligomerization. However, polarized localization in Madin-Darby canine kidney cells was different for homo- and hetero-oligomers. EAAT3 inserts exclusively into apical membranes of Madin-Darby canine kidney cells when expressed alone. Co-expression with EAAT4 results in additional appearance of basolateral EAAT3. Our results demonstrate the existence of heterotrimeric glutamate transporters and provide novel information about the physiological impact of EAAT oligomerization.

Glutamate is the major excitatory neurotransmitter in the mammalian central nervous system. After its release from glutamatergic nerve terminals, glutamate is quickly taken up into glial and neuronal cells by glutamate transporters belonging to the "excitatory amino acid transporter" (EAAT)[4] family (1, 2). Five different mammalian EAAT isoforms have been identified. Two of those, EAAT1 and EAAT2, are expressed mainly in glia, whereas EAAT3, EAAT4, and EAAT5 are considered to be neuronal transporters. All EAAT glutamate transporters sustain two fundamentally distinct transport mechanisms. They function as stoichiometrically coupled co-transporters of one glutamate, three sodium ions, and one proton, while one potassium ion is countertransported (3, 4). In addition, all EAATs are capable of functioning as anion channels (5). Different EAAT isoforms differ in the relative contribution of anion currents to the total transporter-mediated current (5–8). These differences have been interpreted as an indication that some EAATs play a physiological role as glutamate transporters (9, 10) and others as glutamate-gated anion channels involved in the regulation of cellular excitability (2, 11, 12).

EAAT glutamate transporters are assembled as trimers (13–16). At present, it is not clear whether distinct isoforms can form heterotrimers, and moreover, whether subunits might acquire new functions within heterotrimeric assemblies. We here use biochemical and electrophysiological approaches to study co-assembly of different EAATs and possible functional consequences of heteromultimerization.

EXPERIMENTAL PROCEDURES

Heterologous Expression of EAATs—Coding regions of rat EAAT1, human EAAT2, rat and human EAAT3, rat EAAT4, and human SLC26A9 were subcloned into pcDNA3.1 or pRcCMV using PCR-based strategies. YFP, GFP, CFP, and His fusion proteins were generated by PCR-based techniques. All constructs were verified by restriction analysis and DNA sequencing. For each construct, two independent recombinants from the same transformation were examined and shown to exhibit indistinguishable functional properties. Transient transfection of tsA201 and MDCKII cells using the $Ca_3(PO_4)_2$ technique or Lipofectamine (Invitrogen) was performed as described previously (8).

Purification and Gel Electrophoresis of EAAT Fusion Proteins—EAAT fusion proteins were purified from tsA201 cells as described (22). For PAGE under denaturing conditions, proteins were denatured for 15 min at 56 °C with SDS sample buffer containing 20 mM dithiothreitol (DTT) and electrophoresed on linear SDS-polyacrylamide gels. Blue native (BN)-PAGE was performed immediately after protein purification as described (22, 23). YFP-tagged proteins were visualized by scanning the wet polyacrylamide gels with a fluorescence scanner (Typhoon 9400; GE Healthcare). Each

* This work was supported, in whole or in part, by National Institutes of Health Grant R01-NS049335-05 (to C. G.). This work was also supported by Deutsche Forschungsgemeinschaft Grants FA301/6 and 9 (to Ch. F.).

[1] These authors contributed equally to this work.
[2] Present address: Dept. of Neurobiology, University of Pittsburgh, Pittsburgh, PA 15260.
[3] To whom correspondence should be addressed: Institut für Neurophysiologie, Medizinische Hochschule Hannover, Carl-Neuberg-Str. 1, D-30625 Hannover, Germany. Tel.: 49 511 532 2777; Fax: 49 511 532 2776; E-mail: fahlke.christoph@mh-hannover.de.

[4] The abbreviations used are: EAAT, excitatory amino acid transporter; BN, blue native; CFP, cyan fluorescent protein; MDCK, Madin-Darby canine kidney.

experiment was at least performed three times and illustrated as representative result.

Electrophysiology—For expression in oocytes, cRNA was synthesized from MluI-linearized pTLN2-hEAAT3 (24) or from NheI-linearized pGEMHE-R501C rEAAT4 (20) templates through use of MESSAGE machine kits (Ambion, Austin, TX). Injection and handling of oocytes were performed as described elsewhere (25). Current recordings from oocytes expressing hEAAT3 were usually performed 1 day after injection. To account for differences in expression levels, this period was increased to 4–5 days for R501C rEAAT4. For co-expression experiments in oocytes, hEAAT3 and R501C rEAAT4 RNAs were injected at a 1:5 ratio unless otherwise stated.

EAAT-associated currents were recorded by two-electrode voltage clamp using a CA1 amplifier (Dagan, Minneapolis, MN). Oocytes were held at 0 mV, and currents elicited by 200-ms voltage steps between −120 mV and +80 mV were filtered at 2 kHz (−3d B) and digitized with a sampling rate of 10 kHz, using either a Digidata AD/DA converter (Molecular Devices, Sunnyvale, CA) or an ITC-18 Computer Interface (Instrutech Corporation). The external solution contained 96 mM $NaNO_3$, 4 mM KCl, 0.3 mM $CaCl_2$, 1 mM $MgCl_2$, 5 mM HEPES, pH 7.4, either with or without 500 μM L-glutamate or L-serine.

After each experiment with substrate application, the substrate was washed out by perfusion with substrate-free solution and consequently at least once applied again. Cells were only incorporated into the analysis if current amplitudes measured at different times with the same substrate concentration perfectly superimpose. For the experiment shown in Fig. 2, *E–G*, the application order was changed from experiment to experiment.

Laser Pulse Photolysis—Transient transfection of subconfluent human embryonic kidney cell cultures with the calcium phosphate-mediated transfection method and laser pulse photolysis experiments were performed as described previously (26). Electrophysiological recordings were performed 24 h after the transfection for 3 days.

In these experiments, the extracellular solution contained 140 mM NaMES, 2 mM $CaMES_2$, 2 mM $MgMES_2$, and 30 mM HEPES (pH 7.4/NaOH). The pipette solution contained 140 mM NaMES (exchange transport current)/NaSCN (exchange anion current), 2 mM $MgMES_2$, 10 mM EGTA, 10 mM glutamate and serine, and 10 mM HEPES (pH 7.4/NaOH).

Briefly, glutamate or 4-methoxy-7-nitroindolinyl-caged glutamate (Tocris Bioscience, Ellisville, MO) was applied to cells by means of a small quartz tube (350-μm diameter) with a mean velocity of 5 cm/s and a time resolution of 20–30 ms (10–90% rise time with whole cells). Photolysis of caged glutamate was initiated with a light flash (355 nm, 5 ns, frequency-tripled NdYag laser; Continuum, Santa Clara, CA), which was delivered to the cell with an optical fiber (350-μm diameter). Laser energies were varied in the range of 50–450 mJ/cm^2 with neutral density filters. To estimate the concentration of photolytically released glutamate, a standard glutamate concentration of 100 μM was applied to the cells by rapid perfusion before and after photolysis experiments, and the steady-state current amplitude was used to calculate the free glutamate concentration from the dose-response curve (26). Current responses to the laser pulse were low pass-filtered at 3 kHz (100-μs time resolution) and recorded with a 100-kHz sampling rate.

Data Analysis—Data were analyzed with a combination of pClamp9 (Molecular Devices) and SigmaPlot (Jandel Scientific, San Rafael, CA) programs. Current amplitudes were used without applying a subtraction procedure. Current-voltage relationships at various substrate concentrations were constructed by plotting isochronal current amplitudes determined 1 ms after the voltage step *versus* the membrane potential. To obtain the concentration dependence of anion channel activation by Na^+ and glutamate, isochronal anion current amplitudes were measured at various concentrations at a given test potential. The so-obtained substrate dependences were normalized to the maximum current amplitude, fit with Hill equations,

$$\left(I = \frac{I_{max}[\text{substrate}]^n}{[\text{substrate}]^n + {K_D}^n} + I_0 \right) \quad \text{(Eq. 1)}$$

and averaged after normalization to the maximum current amplitude ($I_{max} + I_o$). All data are given as means ± S.E. For statistic evaluation the Student's *t* test was used.

Confocal Microscopy—MDCKII cells were transiently transfected with mCFP-hEAAT3, mYFP-rEAAT4, barttin-YFP, or hSLC26A9-mYFP and grown on Ibidi glass-bottom dishes. Additionally, co-transfections of CFP-hEAAT3/YFP-rEAAT4 and GFP-hEAAT3/mCherry-hEAAT2 were performed (see Fig. 5). Confocal imaging was carried out on living cells with a TCS SP2 AOBS scan head and an inverted Leica DM IRB. CFP was excited at 405 nm, and the emission was detected after filtering with a 450–505 nm bandpass filter. YFP/GFP/mCherry were excited at 514 nm/488 nm/514 nm, and the emission was detected after filtering with 520–580 nm/500–535 nm/555–700 nm bandpass filters, respectively.

Surface Biotinylation and Western Blotting—Cell surface expression of hEAAT3 was assayed with a modification of cell surface biotinylation methods described previously (27, 28). In these experiments, hEAAT3 was expressed as a GFP fusion protein because the fluorescence scanner (Typhoon) had preferable imaging capabilities for GFP. GFP-hEAAT3 alone or GFP-tagged hEAAT3 together with untagged rEAAT4 or hEAAT2 was expressed in MDCKII cells, grown until 70% confluence on filters (see Fig. 6), and incubated with 2 mg/ml biotin (sulfo-NHS-SS-biotin; Pierce) in triethanolamine buffer (2 mM $CaCl_2$, 150 mM NaCl, 10 mM $C_6H_{15}NO_3$, pH 7.5) for 1–2 h, either added to the apical or to the basolateral side. The membrane domain that was not treated with biotin was incubated with biotinylation buffer only. The reaction was quenched by repeated washing with quenching buffer (100 mM glycine in PBS). After washing with PBS, the cells were scraped in lysis buffer (150 mM NaCl, 1% Triton X-100, and 5 mM EDTA with 50 mM Tris, pH 7.5) and transferred to a tube. After 15 min on ice, they were centrifuged at 14,000× *g* for 10 min at 4 °C, and the cell lysate was collected. Cell lysates were incubated with Ultralink immobilized NeutrAvidin beads

(Pierce) for 2 h. After washing with either lysis buffer or high salt wash buffer (0.1% Triton, 500 mM NaCl, 5 mM EDTA, 50 mM Tris, pH 7.5), proteins on the beads were released by incubation with SDS loading buffer containing 200 mM DTT and 4.1% SDS. The proteins were separated on 10% polyacrylamide gradient gels. Fluorescence intensities of apical/basolateral channels were determined by fluorescence scanning and given as fraction of the total surface transporter fluorescence, obtained by adding apical and basolateral fluorescence intensities. Gels were blotted onto polyvinylidene (Bio-Rad), and actin was visualized with rabbit anti-actin antibody (Sigma-Aldrich) and anti-rabbit Cy5 antibody (GE Healthcare). Results were used only from experiments in which no actin was detected in purified membrane fractions. We used heterologously expressed hSLC26A9-YFP as apical (29) and endogenous Na^+,K^+-ATPase as basolateral markers (27). Biotinylated hSLC26A9-YFP was quantified using fluorescent scanning, but we used antibodies (Abcam) and Western blotting for endogenous Na^+,K^+-ATPases.

RESULTS

EAAT3 and EAAT4 Form Hetero-oligomeric Transporters—To study whether different EAAT isoforms assemble into heterotrimeric complexes, we co-expressed two different EAAT isoforms in mammalian cells, one as a YFP fusion protein and the other as a His fusion protein. The tested mammalian EAATs acquire different molecular masses by the distinct added tags and can, thus, be distinguished by gel electrophoresis (Fig. 1*A*). Transporters were either purified in their native multimeric state by Ni^{2+}-nitrilotriacetic acid-based affinity chromatography before gel electrophoresis (eluate fractions) or resolved as full lysates by denaturing SDS- or BN-PAGE (homogenate fractions). YFP-tagged proteins were then visualized by scanning the wet polyacrylamide gels with a fluorescence scanner.

Fig. 1*B* shows a BN-PAGE from cells co-expressing His-hEAAT3 and YFP-rEAAT4 (*lanes 3* and *4*) and from cells expressing each transporter alone (*lanes 1* and *2*). Because His-hEAAT3 homotrimers are not fluorescent, we verified expression of His-hEAAT3 by Western blotting. BN-PAGE of full lysates from cells expressing YFP-rEAAT4 resulted in two different fluorescent bands that correlate to non- or core-glycosylated and complex-glycosylated forms of homotrimers (Fig. 1*B*, *lane 2*) (14). The full homogenate of cells co-transfected with both transporters also contains homotrimeric YFP-rEAAT4 (Fig. 1*B*, *lane 3*). After Ni^{2+}-nitrilotriacetic acid-based affinity chromatography, homotrimeric YFP-rEAAT4, which lacks an affinity tag, is absent from the retained fraction. The protein fraction with the highest molecular mass must represent heterotrimers because it contains the His tag, which is only present in His-hEAAT3, exhibits fluorescence from YFP-rEAAT4, and is of a smaller molecular mass than the YFP-rEAAT4 homotrimer (Fig. 1*B*, *lane 4*, *Eluate*). Fig. 1*C* shows a SDS-PAGE of various fractions isolated from affinity chromatography. Homotrimeric YFP-rEAAT4 does not bind the Ni^{2+} resin and appears completely in the flow-through (*lanes 1–3*). In contrast, heterotrimerization of hEAAT3 and rEAAT4 allows pulldown of YFP-rEAAT4 together with His-hEAAT3 by metal affinity chromatography (Fig. 1*C*, *lanes 4–6*). We used human EAAT3 and rat EAAT4 for these experiments because functional properties of these isoforms were recently studied and compared by our group (25). Although human and rat EAAT3 are highly conserved, they do not exhibit complete sequence identity. To demonstrate that EAAT3/EAAT4 hetero-oligomerization also oc-

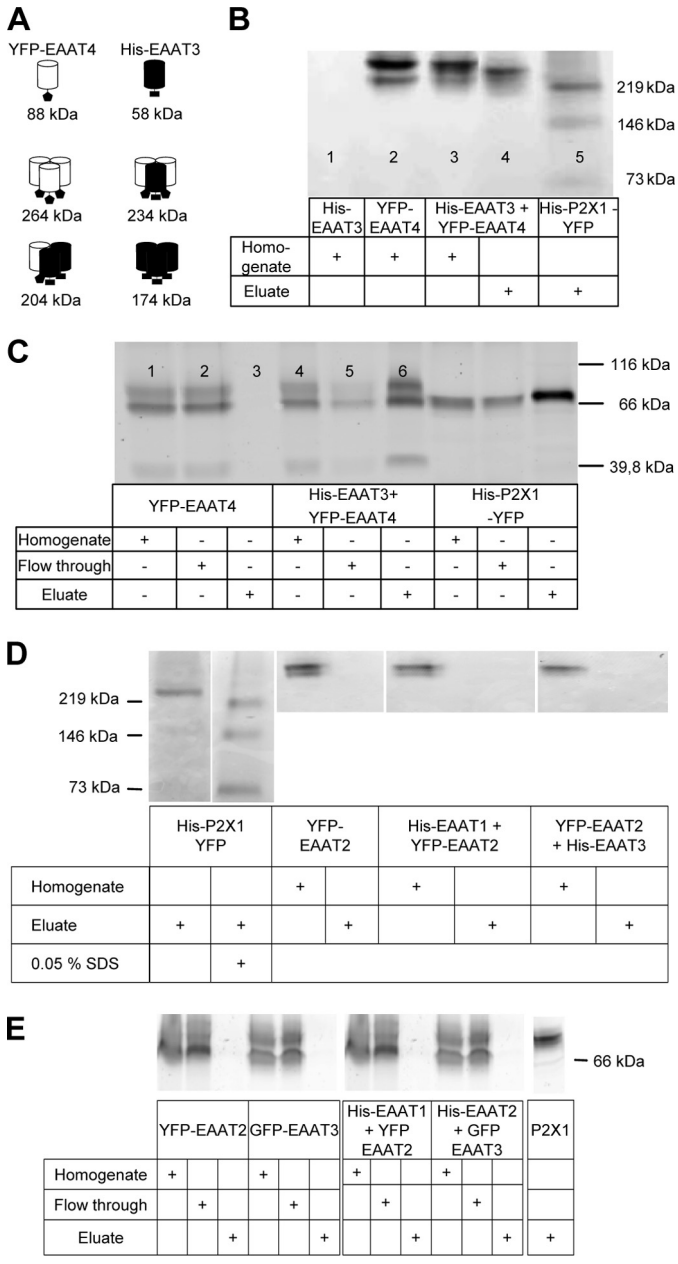

FIGURE 1. **Co-assembly of EAAT3 and EAAT4.** *A*, YFP and His fusion proteins differ in size, allowing distinction of homo- and heterotrimeric proteins by gel electrophoresis. *B*, BN-PAGE of homogenates and eluates from Ni^{2+}-affinity chromatography from cells co-expressing His-EAAT3 and YFP-EAAT4 (*lane 3* and *4*). The trimeric membrane protein P2X1 was used as size standard (*lane 5*). *C*, SDS-PAGE from various fractions obtained by a pull-down assay using Ni^{2+}-affinity chromatography. *D*, BN-PAGE of lysates and eluted proteins after Ni^{2+}-affinity chromatography from cells expressing YFP-hEAAT2 (*third* and *fourth lanes*) or cells co-expressing His-rEAAT1 and YFP-hEAAT2 (*fifth* and *sixth lanes*) as well as His-hEAAT3 and YFP-hEAAT2 (*seventh* and *eighth lanes*). Eluates were concentrated 8-fold. *E*, SDS-PAGE from various fractions obtained by Ni^{2+}-affinity chromatography from cells co-expressing His-rEAAT1 and YFP-hEAAT2, His-hEAAT2 and GFP-hEAAT3.

curs with isoforms from the same species, we repeated co-expression and pulldown experiments with His-rEAAT3 and YFP-rEAAT4. The outcome of these experiments closely resembled those with hEAAT3 and rEAAT4 (data not shown). YFP-rEAAT4 and His-rEAAT3 form heterotrimers.

We conclude that EAAT3 and EAAT4 can co-assemble into heteromultimers. Other isoforms fail to co-assemble (Fig. 1, *D* and *E*). Neither BN-PAGE analysis (Fig. 1*D*) nor pull-down assays (Fig. 1*E*) revealed any indication for hetero-oligomerization for three other EAAT isoform combinations, the two glial transporters EAAT1 and EAAT2 as well as for EAAT2 and EAAT3.

Co-expression of EAAT3 and EAAT4 in Xenopus Oocytes—hEAAT3 and rEAAT4 differ in the unitary glutamate transport rate (30) but not in the unitary anion current (25). Moreover, macroscopic anion currents display isoform-specific time and voltage dependences (25). hEAAT3/rEAAT4 heterotrimers therefore provide an excellent possibility to study potential intersubunit interactions. To separate currents conducted by hEAAT3 or rEAAT4 subunits, we mutated rEAAT4 at position 501 (R501C) to modify the substrate binding pocket in a way that glutamate cannot bind anymore, but serine or cysteine can bind instead (17, 20, 31).

Fig. 2 shows current recordings from *Xenopus* oocytes expressing either WT hEAAT3 or R501C rEAAT4 alone, or co-expressing both isoforms. In the presence of extracellular NO_3^- these currents are dominated at positive membrane potentials by the anion component (8, 32, 33).

When the membrane potential is stepped to more positive values, WT hEAAT3 currents display time- and voltage-dependent increases (Fig. 2*A*, *arrow*), likely due to channel activation (25). In contrast R501C rEAAT4, like WT rEAAT4, is inactivated by positive voltages (Fig. 2*B*) (8, 20, 25), resulting in decreased channel open probabilities and time-dependent current amplitude reductions (*arrow*) (8, 25, 34). WT hEAAT3 currents are greatly increased in the presence of extracellular glutamate, but are not responsive to serine (Fig. 2*A*). In contrast, R501C rEAAT4 currents are not significantly affected by glutamate, but they are augmented by application of extracellular serine (Fig. 2*B*).

Fig. 2, *C* and *D*, shows the time course of the development of glutamate- and serine-dependent currents with time after mRNA injection. Serine-dependent anion currents are larger in oocytes co-expressing WT hEAAT3 and R501C rEAAT4 than in those expressing R501C rEAAT4 alone (Fig. 2*D*), indicating that hEAAT3 stimulates the insertion of rEAAT4 subunits into the surface membrane. Confocal images from oocytes expressing YFP-rEAAT4 alone or co-expressing YFP-rEAAT4 and untagged hEAAT3 revealed increased surface insertion of YFP-rEAAT4 in the presence of hEAAT3 (data not shown). In contrast, expression of R501C rEAAT4 did not increase glutamate-dependent hEAAT3 anion currents, but rather decrease this current amplitude at certain time intervals (Fig. 2*C*).

Fig. 2*E* shows representative recordings from a single co-injected oocyte and the corresponding analysis. Currents were measured in the absence as well as in the presence of glutamate and serine. For the application of each substrate alone as well as for the simultaneous application of both, we determined substrate-dependent current amplitudes for various voltages and constructed current-voltage relationships from these data (Fig. 2*F*). Current increases elicited by the simultaneous presence of glutamate and serine were slightly smaller than the sums of the current amplitudes induced by only one substrate at positive potentials (Fig. 2*G*). At negative potentials, where current amplitudes are dominated by coupled

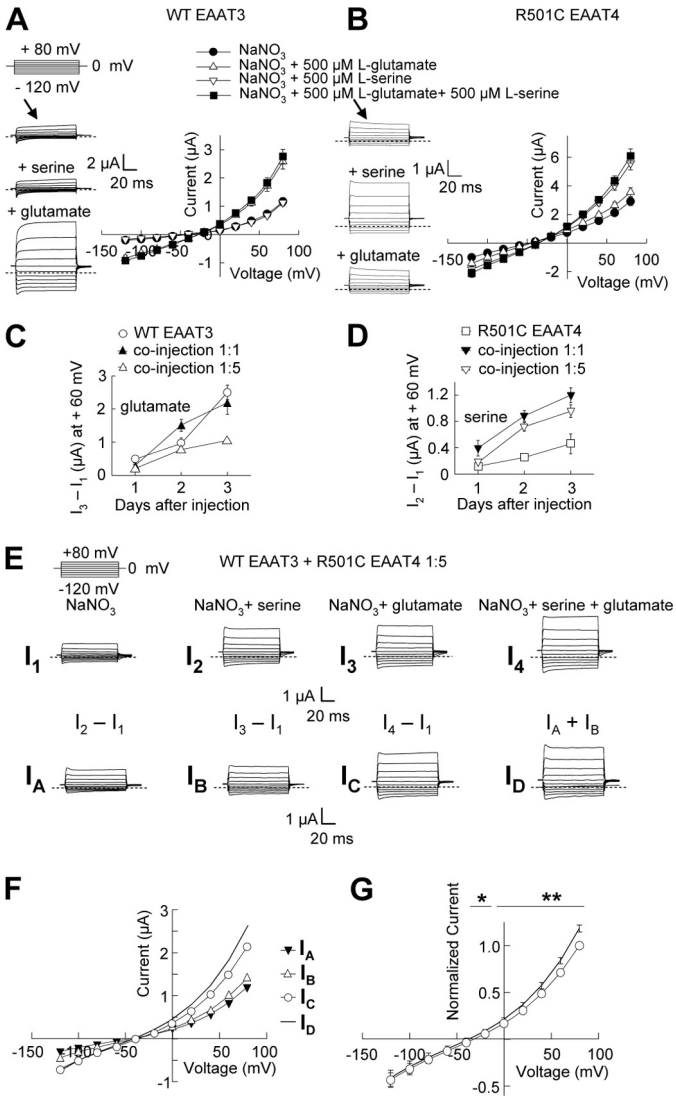

FIGURE 2. **EAAT3 modifies membrane surface insertion and function of EAAT4.** *A* and *B*, representative recordings and current-voltage relationships from oocytes expressing WT EAAT3 (*A*) or R501C EAAT4 (*B*) in the following conditions, 96 mM $NaNO_3$ (*filled circles*), 96 mM $NaNO_3$ + 500 μM L-glutamate (*upward triangles*), and 96 mM $NaNO_3$ + 500 μM L-serine (*downward triangles*). Mean ± S.E. from 6–7 experiments is shown. *C* and *D*, dependences of the glutamate-induced (*C*) and serine-induced (*D*) currents on the time after mRNA injection for oocytes expressing WT EAAT3 ($n = 8$ for each time point), R501C EAAT4 ($5 < n > 10$), and oocytes co-expressing WT EAAT3 and R501C EAAT4 ($5 < n > 10$) at different ratios. *E*, representative recordings from an oocyte co-expressing hEAAT3 and R501C rEAAT4 without substrate (I_1) in the presence of 96 mM $NaNO_3$ + 500 μM L-serine (I_2) or 500 μM L-glutamate (I_3), or after application of both (I_4). *F*, current-voltage relationship for serine-activated ($I_A = I_2 - I_1$) and glutamate-activated ($I_B = I_3 - I_1$) currents as well as of currents activated in the simultaneous presence of serine and glutamate ($I_C = I_4 - I_1$) from the example shown in *E*. The *solid line* gives the sum of serine- and glutamate-activated current amplitudes. *G*, averaged normalized current-voltage relationship for different substrate-sensitive current components ($n = 6$, *, $p < 0.05$; **, $p < 0.01$).

transport currents, no difference between the two amplitudes could be observed (Fig. 2*G*).

Individual Subunits Transport Substrates Independently of Each Other—WT hEAAT3 and R501C rEAAT4 differ in the apparent dissociation constants for glutamate/serine and sodium (25, 30). To test whether binding of an amino acid substrate/cation to one subunit is affected by the neighboring subunit, we determined glutamate concentration dependences of hEAAT3 anion currents when expressed alone or co-expressed together with R501C rEAAT4 in oocytes (Fig. 3*A*), or serine concentration dependences of R501C rEAAT4 currents either expressed alone or co-expressed with WT hEAAT3 (Fig. 3*B*). No differences in the apparent dissociation constants were observed. Moreover, the serine concentration dependence was not affected when co-applied with a saturating concentration of glutamate (Fig. 3, *C* and *D*), a condition in which the hEAAT3 is expected to be predominantly in the inward-facing, but not in the outward-facing configuration.

At saturating glutamate (Fig. 3*E*) or serine concentrations (Fig. 3*F*), WT hEAAT3 and R501C rEAAT4 differ significantly in the apparent dissociation constants for sodium, with R501C rEAAT4 showing significantly higher apparent affinity. However, co-expression of the two transporters does not modify sodium binding (Fig. 3, *E* and *F*).

To test for potential subunit interactions during coupled substrate transport, we employed heterologous expression in mammalian cells and rapid application of glutamate with subsequent analysis of the relaxation of the transport-associated currents. This approach allows the resolution of early conformational changes in glutamate transporters (Fig. 4). Because homotrimeric R501C rEAAT4s are insensitive to glutamate, differences in current responses of cells co-expressing WT hEAAT3 and R501C rEAAT4 from cells expressing hEAAT3 alone will indicate modification of the function of hEAAT3 by adjacent rEAAT4 subunits. We performed these experiments under two different intracellular ionic conditions, *i.e.* with MES^- or with SCN^- as the predominant intracellular anion. In both types of experiments, intracellular K^+ was replaced by Na^+, eliminating the relocation of the K^+-bound transporter. With internal MES^-, there are no contributions of EAAT anion channels, and currents reflect conformational changes in the Na^+/glutamate homoexchange mode (33) (Fig. 4, *A* and *B*). SCN^- represents the anion with highest permeability through the EAAT anion pore (8, 25, 32), and in cells dialyzed with internal SCN^-, currents at negative potentials are dominated by EAAT-mediated anion currents.

Two kinetic components of the current signal in response to glutamate application are observed in hEAAT3-expressing cells, a fast component due to Na^+ binding and a conformational change subsequent to the association of glutamate with the transporter (35) and a slow component representing the translocation of Na^+ and glutamate (26). Homo- and heterotrimeric transporters display identical time constants and relative amplitudes of the two kinetic components (Fig. 4*B*). The two kinetic processes can also be observed in the presence of internal SCN^-. In this case, sudden increases of the external glutamate concentration result in a biexponential activation of hEAAT3 anion channels with the same time constants as

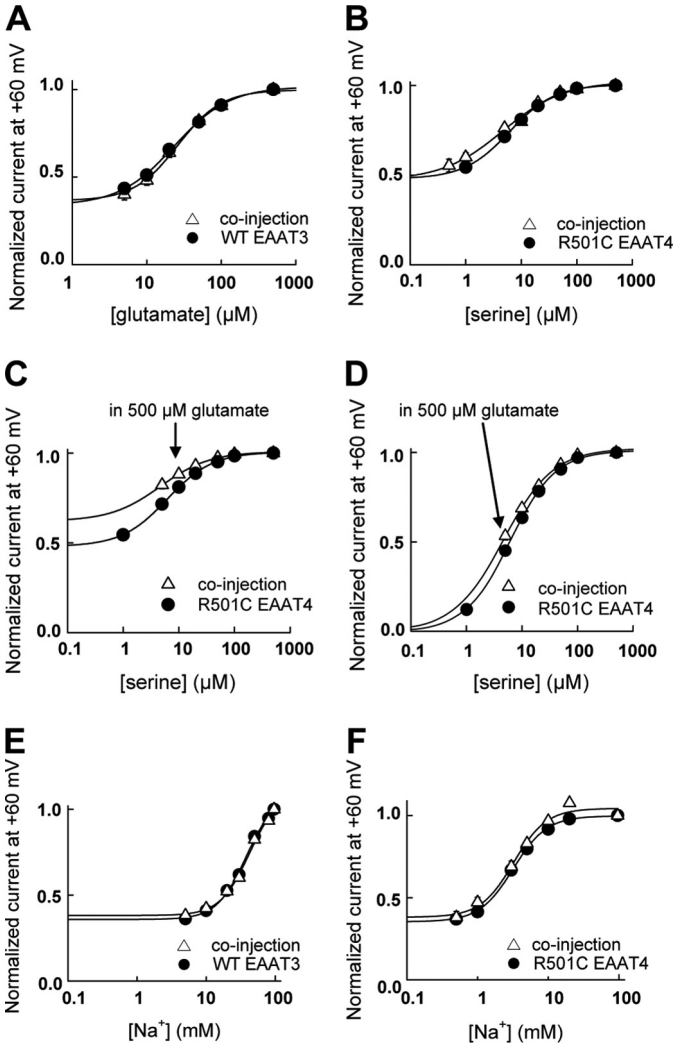

FIGURE 3. **Substrates bind independently to individual subunits.** *A*, glutamate dependence of isochronal current amplitudes measured at +60 mV from oocytes expressing WT EAAT3 (*filled circles*, $n = 3$, $K_D = 23.4 \pm 1.2$ μM) and oocytes co-expressing WT EAAT3 and R501C EAAT4 (*open triangles*, $n = 6$, $K_D = 26.0 \pm 2.4$ μM) in the absence of serine. *B*, serine dependence of isochronal current amplitudes from oocytes expressing R501C EAAT4 (*filled circles*, $n = 3$, $K_D = 6.1 \pm 0.1$ μM) or co-expressing WT EAAT3 and R501C EAAT4 (*open triangles*, $n = 6$, $K_D = 4.6 \pm 0.7$ μM) in the absence of glutamate. *C*, comparison of the serine dependence of isochronal current amplitudes from oocytes expressing R501C EAAT4 (shown in *B*) with the serine dependence from oocytes co-expressing WT EAAT3 and R501C EAAT4 in the presence of 500 μM glutamate (*open triangles*, $n = 5$, $K_D = 4.6 \pm 0.2$ μM). *D*, serine dependence of substrate-dependent anion current amplitudes. Data from *C* were scaled by setting the minimum values to 0 and the maximum values to 1. *E*, sodium dependence of isochronal current amplitudes from oocytes expressing WT EAAT3 (*filled circles*, $n = 5$, $K_D = 38.2 \pm 0.8$ mM) and oocytes co-expressing WT EAAT3 and R501C EAAT4 (*open triangles*, $n = 8$, $K_D = 42.5 \pm 0.5$ mM) in the presence of 500 μM L-glutamate. *F*, sodium dependence of the isochronal current amplitude from oocytes expressing R501C EAAT4 (*closed circles*, $n = 6$, $K_D = 6.4 \pm 1.4$ mM) or co-expressing WT EAAT3 and R501C EAAT4 (*open triangles*, $n = 4$, $K_D = 5.5 \pm 0.5$ mM) in the presence of 500 μM L-serine.

observed in the absence of permeant anions (Fig. 4, *C* and *D*). Serine activates R501C rEAAT4 anion channels and thus increases the current amplitude in cells expressing heterotrimers in the presence of internal SCN^-. However, the rate constants of current activation were not affected by the co-expression of R501C rEAAT4, either in the absence or in the presence of serine (Fig. 4, *E* and *F*). We conclude that, within

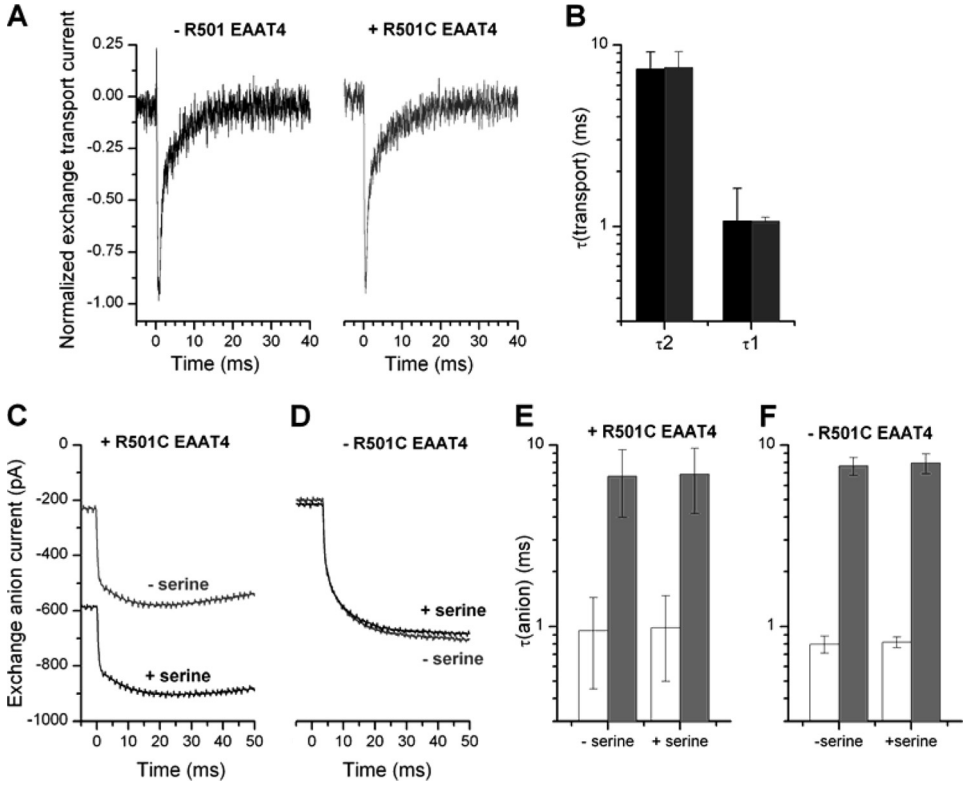

FIGURE 4. **Substrate translocation occurs independently by individual subunits.** *A*, typical exchange transport current recordings (in the absence of permeating anions) after laser pulse photolytic release of glutamate at $t = 0$ with cells expressing WT EAAT3 alone or co-expressing WT EAAT3 and R501C EAAT4 (internal solution contained 140 mM NaMES and 10 mM glutamate and serine, exchange mode). The presence of R501C EAAT4 was tested by applying a saturating serine concentration in the anion-conducting mode. The decay of the transport current is biphasic in both cases and could be fit with a sum of two exponentials, yielding two time constants. *B*, quantification of the time constants associated with the rapidly and slowly decaying phases of the exchange transport current for WT EAAT3-expressing cells (*black*, $n = 3$) and R501C EAAT4 + WT EAAT3-expressing cells (*grey*, $n = 3$). *C* and *D*, typical anion current recordings (inward current caused predominantly by outflow of the highly permeant anion SCN^-) after laser pulse photolytic release of glutamate at $t = 0$ with cells expressing WT EAAT3 alone or co-expressing WT EAAT3 and R501C EAAT4 in the absence (*grey traces*) and presence (*black traces*) of serine (internal solution contained 140 mM NaSCN and 10 mM glutamate and serine, exchange mode). In *C*, the baseline current of the *black trace* is increased due to the continuous presence of serine, preactivating R501C EAAT4. In the absence of R501C EAAT4, serine had no effect. The rise of the current was fit with a sum of two exponentials, yielding two time constants. *E* and *F*, quantification of the time constants associated with the rapidly (*open bars*) and slowly (*gray bars*) rising phases of the exchange anion current for R501C EAAT4 + WT EAAT3-expressing cells (*E*, $n = 3$) and WT EAAT3-expressing cells (*F*, $n = 3$) in the presence and absence of extracellular serine. *Error bars*, S.D.

heterotrimeric assemblies, individual EAAT subunits bind and transport amino acid substrates and sodium ions independently of each other.

Targeting of Heterotrimeric Transporters in Polarized Epithelial Cells—EAAT3 exhibits a unique sorting signal that targets transporters to the apical membrane of epithelial cells and into neuronal dendrites (27). EAAT1, EAAT2, and EAAT4 lack this signal and are therefore distributed differently in MDCK cells than hEAAT3 (27). We used co-expression of fluorescent protein-tagged hEAAT3 and rEAAT4, confocal imaging (Fig. 5) and surface biotinylation (Fig. 6) to study whether heterotrimerization affects epithelial sorting. We first performed confocal imaging in confluent monolayers to study alteration of epithelial sorting (Fig. 5). Whereas CFP-hEAAT3 alone is predominantly inserted into the apical dome (Fig. 5*A*), YFP-rEAAT4 is visible in the apical and in the basolateral membranes (Fig. 5*B*). We used barttin as basolateral (28, 36) (Fig. 5*C*) and SLC26A9 as apical marker (Fig. 5*D*) (29). Co-transfection of CFP-hEAAT3 and YFP-rEAAT4 results in the appearance of hEAAT3 and rEAAT4 in apical as well as in basolateral (*arrows*) domains (Fig. 5*E*). As expected for hetero-oligomerizing subunits, YFP and CFP fluorescence co-localizes. In contrast, co-transfection of GFP-hEAAT3 with mCherry-hEAAT2 that does not result in the formation of heterotrimers (Fig. 1) fails to route hEAAT3 to the basolateral domain (Fig. 5*F*, *arrows*).

To quantify this alteration of epithelial sorting, we performed surface biotinylation in confluent monolayers of MDCK cells grown on filters (Fig. 6). Fig. 6*A* displays the fluorescent scan of a SDS-polyacrylamide gel with purified membrane-inserted GFP-hEAAT3 after biotin application to the apical or the basolateral site of cells expressing GFP-hEAAT3 alone or co-expressing GFP-hEAAT3 and rEAAT4 or hEAAT2. In all cases, the majority of biotinylated EAAT3 protein is complex-glycosylated. Endogenous Na^+,K^+-ATPase and hSLC26A9-YFP were used as basolateral or apical controls.

Fig. 6*B* shows the relative amounts of biotinylated GFP-hEAAT3 after biotin application to the apical or the basolateral site, when expressed alone or co-expressed with nonfluorescent rEAAT4. Whereas hEAAT3 homotrimers preferentially inserts into the apical membrane, heterotrimerization results in equal distribution of hEAAT3 in the apical and the basolateral membrane. Co-expression with hEAAT2 does not modify the polarized expression of hEAAT3 (Fig. 6*C*). We conclude that hEAAT3 is targeted to distinct regions as homotrimer or as a hEAAT3/rEAAT4 heterotrimer.

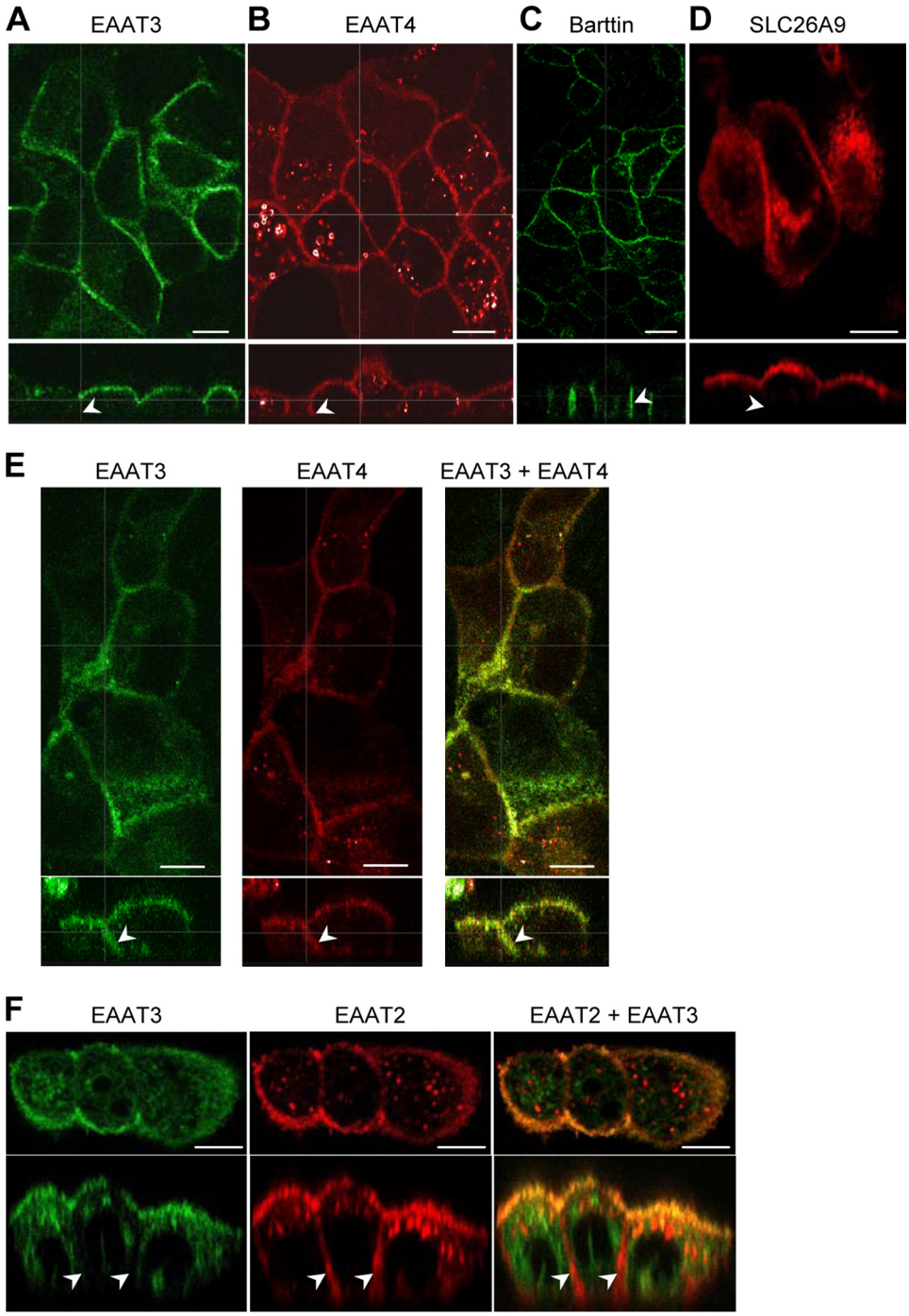

FIGURE 5. **Epithelial sorting of homo- and heterotrimeric EAATs observed by confocal imaging.** *A–D*, confocal images of MDCK cells that transiently express CFP-hEAAT3 (*A*), YFP-rEAAT4 (*B*), barttin-YFP (*C*), or hSLC26A9-YFP (*D*). *E*, co-expression of CFP-EAAT3 and YFP-rEAAT4. CFP is shown in *green*, and YFP is shown in *red*. This color code results in an *orange* coloring of regions where both proteins overlap. Individual YFP and CFP fluorescences are added to demonstrate co-localization of hEAAT3 and rEAAT4. *F*, co-expression of GFP-hEAAT3 and mCherry-hEAAT2. GFP is shown in *green*, and mCherry is shown in *red*. GFP and mCherry fluorescences are added to demonstrate co-localization of hEAAT3 and hEAAT2. *Arrows* indicate basolateral membranes. *x-y* projections (front view) are given in the *upper part*, *x-z* projections (side view) in the *lower part*. *Scale bar*, 5 μm.

DISCUSSION

We here demonstrate that EAAT3 and EAAT4, but neither EAAT1 and EAAT2 nor EAAT2 and EAAT3, co-assemble into stable heterotrimers in heterologous expression systems. EAAT3 and EAAT4 co-express in several cell types of the mammalian brain (37, 38), and heterotrimers might, thus, represent a significant portion of the native transporters. BN-PAGE demonstrates the existence of stable heterotrimers, providing compelling evidence for a direct interaction of EAAT3 and EAAT4 (Fig. 1). There are no indications for dimers and monomers or for higher order oligomers, *i.e.* the linkage of two trimers via interacting proteins.

Recent reports have demonstrated that co-expression of WT and mutant EAAT subunits results in a superposition of

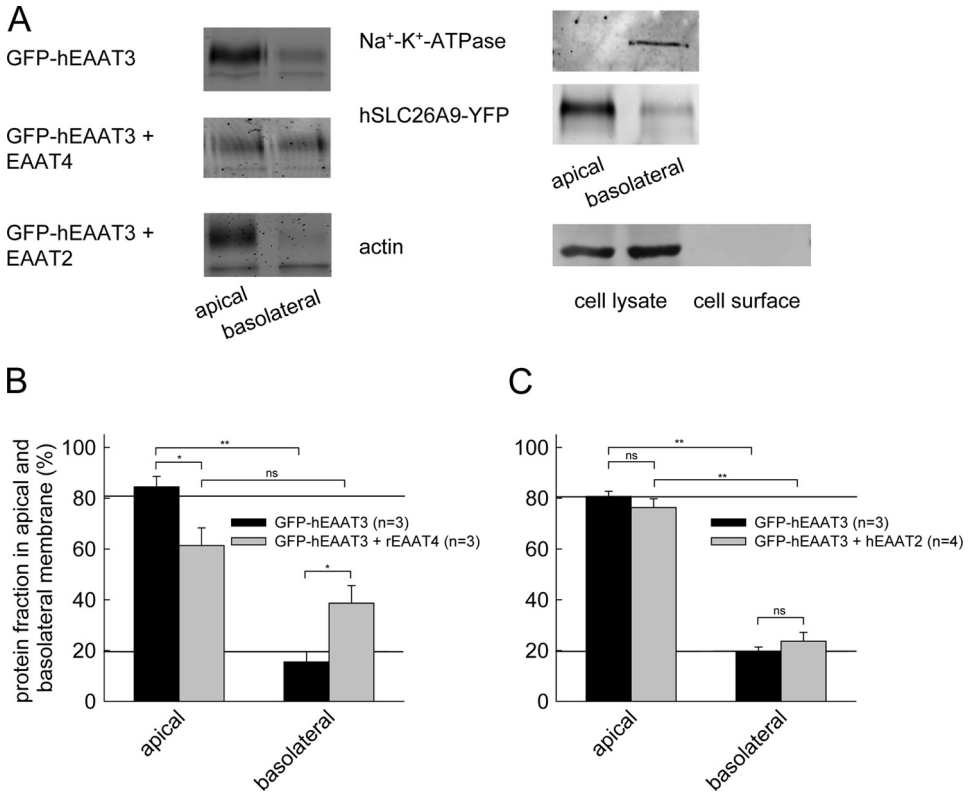

FIGURE 6. **Epithelial sorting of homo- and heterotrimeric EAATs studied by cell surface biotinylation.** *A*, fluorescent scans of SDS-PAGE of GFP-hEAAT3 purified by surface biotinylation from basolateral and apical membranes of MDCK cells expressing GFP-hEAAT3 alone or together with untagged rEAAT4 or hEAAT2. Control blots show that Na^+,K^+-ATPase is detected at the basolateral but not the apical cell surface fraction, whereas heterologously expressed SLC26A9-mYFP is predominantly present in the apical membrane. Actin was only detected in the intracellular fraction. *B* and *C*, relative amounts of EAAT3 protein in the apical and the basolateral membrane when expressed alone or together with rEAAT4 (*B*) or hEAAT2 (*C*). GFP-EAAT3 was surface-biotinylated from the apical or the basolateral membrane, quantified by GFP fluorescence, and given as relative amount of the total surface fluorescence. Data represent means ± S.E. (*error bars*) from three experiments. Level of significance: *, $p < 0.05$; **, $p < 0.01$. *Solid lines* give the proportion of the apical marker protein hSLC26A9 in basolateral or apical fractions.

WT and mutant glutamate transport and anion currents, in full agreement with functionally independent subunits (17–19). We extended these studies by measuring substrate dependences (Fig. 3) as well as early conformational changes (Fig. 4) in heterotrimeric glutamate transporters. Our results support the idea that individual subunits function independently within the hetero-oligomeric assembly. The substrate concentration dependences of hEAAT3 and R501C rEAAT4 anion currents are similar in homo- and in heterotrimeric assemblies (Fig. 3). Pre-steady-state kinetics of hEAAT3 are unaffected by the presence of R501C rEAAT4 in the heteromultimer (Fig. 4). Co-expression of hEAAT3 and serine-sensitive R501C rEAAT4 results in uptake currents that are identical to the superposition of currents mediated by hEAAT3 and R501C rEAAT4 (Fig. 2*G*). For EAAT-associated anion currents, we observed slight deviations from the expectations of complete independence of individual subunits (Fig. 2*G*).

Structural evidence from the bacterial EAAT homolog Glt_{Ph} (39) suggested that substrate transport requires a major conformational change. Comparison of high resolution structures of Glt_{Ph} in the outward-facing (15) and in the inward-facing conformation (39) demonstrated a largely immobile "trimerization domain" (containing TM1, TM2, TM4, and TM5) and a "transport domain" undergoing substantial movements during the glutamate transport process (39). This transport mechanism requires trimerization for normal transport and suggests that monomeric Glt_{Ph} subunits might be unable to transport, in contrast to other multimeric transporter families (40). The apparent independence of EAAT subunits indicates that any transmission of conformational changes to other subunits through the trimerization domain may be minor.

Neither the glial transporters EAAT1 and EAAT2 nor EAAT2 and EAAT3 or EAAT2 and EAAT4 have the ability to co-assemble (Fig. 1). Heterotrimerization is, therefore, not a common feature of different EAAT isoforms. At present, we can only speculate about the biological significance of the hetero-oligomerization of EAAT3 and EAAT4. EAAT3 and EAAT4 are co-expressed in certain neurons of the central nervous system. Cooperation of different targeting signals might result in the insertion of heteromultimers in cell regions that exclude homotrimers. Heterotrimerization results in close proximity of low affinity/high capacity (EAAT3) and high affinity/low capacity (EAAT4) transporter (30), allowing tight regulation of the external glutamate concentration. Because EAAT anion channels possibly modulate neuronal excitability (2, 11), relative expression levels of EAAT3 and EAAT4 will result in distinct pattern of neuronal excitability and its regulation by glutamate.

Acknowledgments—We thank Dr. M. Hediger, Dr. J. Rothstein, Dr. T. Rauen, Dr. W. Stoffel, Dr. Rainer Schreiber, and Dr. Karl Kunzelmann for providing the expression constructs for hEAAT2, hEAAT3, rEAAT4, rEAAT3, rEAAT1, and hSLC26A9; Dr. Patricia Hidalgo for helpful discussions; and Birgit Begemann for excellent technical assistance.

REFERENCES

1. Danbolt, N. C. (2001) *Prog. Neurobiol.* **65,** 1–105
2. Amara, S. G., and Fontana, A. C. (2002) *Neurochem. Int.* **41,** 313–318
3. Levy, L. M., Warr, O., and Attwell, D. (1998) *J. Neurosci.* **18,** 9620–9628
4. Zerangue, N., and Kavanaugh, M. P. (1996) *Nature* **383,** 634–637
5. Wadiche, J. I., Amara, S. G., and Kavanaugh, M. P. (1995) *Neuron* **15,** 721–728
6. Fairman, W. A., Vandenberg, R. J., Arriza, J. L., Kavanaugh, M. P., and Amara, S. G. (1995) *Nature* **375,** 599–603
7. Watzke, N., and Grewer, C. (2001) *FEBS Lett.* **503,** 121–125
8. Melzer, N., Biela, A., and Fahlke, Ch. (2003) *J. Biol. Chem.* **278,** 50112–50119
9. Tanaka, K., Watase, K., Manabe, T., Yamada, K., Watanabe, M., Takahashi, K., Iwama, H., Nishikawa, T., Ichihara, N., Kikuchi, T., Okuyama, S., Kawashima, N., Hori, S., Takimoto, M., and Wada, K. (1997) *Science* **276,** 1699–1702
10. Watase, K., Hashimoto, K., Kano, M., Yamada, K., Watanabe, M., Inoue, Y., Okuyama, S., Sakagawa, T., Ogawa, S., Kawashima, N., Hori, S., Takimoto, M., Wada, K., and Tanaka, K. (1998) *Eur. J. Neurosci.* **10,** 976–988
11. Melzer, N., Torres-Salazar, D., and Fahlke, Ch. (2005) *Proc. Natl. Acad. Sci. U.S.A.* **102,** 19214–19218
12. Veruki, M. L., Mørkve, S. H., and Hartveit, E. (2006) *Nat. Neurosci.* **9,** 1388–1396
13. Haugeto, O., Ullensvang, K., Levy, L. M., Chaudhry, F. A., Honoré, T., Nielsen, M., Lehre, K. P., and Danbolt, N. C. (1996) *J. Biol. Chem.* **271,** 27715–27722
14. Gendreau, S., Voswinkel, S., Torres-Salazar, D., Lang, N., Heidtmann, H., Detro-Dassen, S., Schmalzing, G., Hidalgo, P., and Fahlke, Ch. (2004) *J. Biol. Chem.* **279,** 39505–39512
15. Yernool, D., Boudker, O., Jin, Y., and Gouaux, E. (2004) *Nature* **431,** 811–818
16. Koch, H. P., and Larsson, H. P. (2005) *J. Neurosci.* **25,** 1730–1736
17. Grewer, C., Balani, P., Weidenfeller, C., Bartusel, T., Tao, Z., and Rauen, T. (2005) *Biochemistry* **44,** 11913–11923
18. Leary, G. P., Stone, E. F., Holley, D. C., and Kavanaugh, M. P. (2007) *J. Neurosci.* **27,** 2938–2942
19. Koch, H. P., Brown, R. L., and Larsson, H. P. (2007) *J. Neurosci.* **27,** 2943–2947
20. Torres-Salazar, D., and Fahlke, C. (2006) *J. Neurosci.* **26,** 7513–7522
21. Deleted in proof
22. Detro-Dassen, S., Schänzler, M., Lauks, H., Martin, I., zu Berstenhorst, S. M., Nothmann, D., Torres-Salazar, D., Hidalgo, P., Schmalzing, G., and Fahlke, Ch. (2008) *J. Biol. Chem.* **283,** 4177–4188
23. Nicke, A., Bäumert, H. G., Rettinger, J., Eichele, A., Lambrecht, G., Mutschler, E., and Schmalzing, G. (1998) *EMBO J.* **17,** 3016–3028
24. Trotti, D., Peng, J. B., Dunlop, J., and Hediger, M. A. (2001) *Brain Res.* **914,** 196–203
25. Torres-Salazar, D., and Fahlke, Ch. (2007) *J. Biol. Chem.* **282,** 34719–34726
26. Watzke, N., Bamberg, E., and Grewer, C. (2001) *J. Gen. Physiol.* **117,** 547–562
27. Cheng, C., Glover, G., Banker, G., and Amara, S. G. (2002) *J. Neurosci.* **22,** 10643–10652
28. Janssen, A. G., Scholl, U., Domeyer, C., Nothmann, D., Leinenweber, A., and Fahlke, Ch. (2009) *J. Am. Soc. Nephrol.* **20,** 145–153
29. Lohi, H., Kujala, M., Makela, S., Lehtonen, E., Kestila, M., Saarialho-Kere, U., Markovich, D., and Kere, J. (2002) *J. Biol. Chem.* **277,** 14246–14254
30. Mim, C., Balani, P., Rauen, T., and Grewer, C. (2005) *J. Gen. Physiol.* **126,** 571–589
31. Bendahan, A., Armon, A., Madani, N., Kavanaugh, M. P., and Kanner, B. I. (2000) *J. Biol. Chem.* **275,** 37436–37442
32. Wadiche, J. I., and Kavanaugh, M. P. (1998) *J. Neurosci.* **18,** 7650–7661
33. Grewer, C., Watzke, N., Wiessner, M., and Rauen, T. (2000) *Proc. Natl. Acad. Sci. U.S.A.* **97,** 9706–9711
34. Kovermann, P., Machtens, J. P., Ewers, D., and Fahlke, Ch. (2010) *J. Biol. Chem.* **285,** 23676–23686
35. Mim, C., Tao, Z., and Grewer, C. (2007) *Biochemistry* **46,** 9007–9018
36. Estévez, R., Boettger, T., Stein, V., Birkenhäger, R., Otto, E., Hildebrandt, F., and Jentsch, T. J. (2001) *Nature* **414,** 558–561
37. Furuta, A., Rothstein, J. D., and Martin, L. J. (1997) *J. Neurosci.* **17,** 8363–8375
38. Furuta, A., Martin, L. J., Lin, C. L., Dykes-Hoberg, M., and Rothstein, J. D. (1997) *Neuroscience* **81,** 1031–1042
39. Reyes, N., Ginter, C., and Boudker, O. (2009) *Nature* **462,** 880–885
40. Robertson, J. L., Kolmakova-Partensky, L., and Miller, C. (2010) *Nature* **468,** 844–847